Construction, imaging, and analysis of FRET-based tension sensors in living cells

Andrew S. LaCroix*, Katheryn E. Rothenberg*, Matthew E. Berginski, Aarti N. Urs, Brenton D. Hoffman[1]

Department of Biomedical Engineering, Duke University, Durham, North Carolina, USA
[1]Corresponding author: E-mail: bdh24@duke.edu

CHAPTER OUTLINE

*These authors contributed equally to this work.

Methods in Cell Biology, Volume 125, ISSN 0091-679X, http://dx.doi.org/10.1016/bs.mcb.2014.10.033

Abstract

Due to an increased appreciation for the importance of mechanical stimuli in many biological contexts, an interest in measuring the forces experienced by specific proteins in living cells has recently emerged. The development and use of Förster resonance energy transfer (FRET)-based molecular tension sensors has enabled these types of studies and led to important insights into the mechanisms those cells utilize to probe and respond to the mechanical nature of their surrounding environment. The process for creating and utilizing FRET-based tension sensors can be divided into three main parts: construction, imaging, and analysis. First we review several methods for the construction of genetically encoded FRET-based tension sensors, including restriction enzyme-based methods as well as the more recently developed overlap extension or Gibson Assembly protocols. Next, we discuss the intricacies associated with imaging tension sensors, including optimizing imaging parameters as well as common techniques for estimating artifacts within standard imaging systems. Then, we detail the analysis of such data and describe how to extract useful information from a FRET experiment. Finally, we provide a discussion on identifying and correcting common artifacts in the imaging of FRET-based tension sensors.

INTRODUCTION

Over the past several decades, interest has developed in the mechanical nature of living cells. Initial efforts, guided by the importance of cell migration in many pathological and pathophysiological settings, focused on the ability of cells to generate forces. Some notable achievements include the visualization of cell force generation through the wrinkling of silicon rubber substrata (Harris, Wild, & Stopak, 1980) as well as the quantification of these forces through traction force microscopy, which can be based on deformable hydrogels (Dembo & Wang, 1999), micropatterned substrates (see Martiel et al., [Chapter 15 of this volume]), or microfabricated devices (Tan et al., 2003) (see also Gupta et al., [Chapter 16 of this volume]). Recently, these techniques have been extended to reproducibly measure cellular force generation with spatial resolutions on the order of microns and sub-second temporal resolution (Plotnikov, Pasapera, Sabass, & Waterman, 2012) and have been used to measure forces generated by cells in migrating layers (see Serra-Picamal et al., [Chapter 17 of this volume]) as well as in three dimensional cell culture systems (Legant et al., 2010).

Lately, interest has emerged in determining the mechanisms those cells use to detect and respond to mechanical stimulation. This occurs through a poorly understood process, termed mechanotransduction, by which mechanical stimuli are converted into biochemically detectable signals (Hoffman, Grashoff, & Schwartz, 2011; Orr, Helmke, Blackman, & Schwartz, 2006). This conversion is thought to involve force-induced changes in protein conformation, exposing cryptic binding or signaling domains that are inaccessible to other proteins in the unloaded

conformation. This was directly demonstrated for the focal adhesion proteins talin and vinculin using an in vitro system comprised of purified proteins (del Rio et al., 2009). This, and many other interesting results, led to an interest in visualizing and quantifying the forces experienced by specific proteins in living cells.

Measurements of molecular-scale deformations in living cells were made possible by the development of biosensors based on Förster resonance energy transfer (FRET) (Grashoff et al., 2010; Meng, Suchyna, & Sachs, 2008). FRET is a process by which energy is nonradiatively transferred between an excited donor fluorophore and an adjacent acceptor fluorophore (Lakowicz, 2006). The amount of FRET that occurs is sensitive to the optical properties, relative orientation, mobility, and, importantly, the separation distance of the fluorophores. By assuming that the fluorophores diffuse randomly and have no preferred orientation, the FRET efficiency (E) can be described by the simple equation $E = R_o^6/(R_o^6 + r^6)$. Where, R_o is the Förster distance, or the fluorophore separation distance where 50% FRET efficiency is achieved, and r is the separation distance of the two fluorophores (Lakowicz, 2006). Recently, a number of groups have created biosensors which take advantage of this relationship between force, extension, and FRET to measure the tension across a protein of interest (Hoffman, 2014). These FRET-based tension sensors allow for the measurement of forces in specific subcellular structures, and have provided novel insights into the complex processes underlying mechanotransduction. Here we focus on the design, construction, validation, and use of FRET-based tension sensors.

1. DESIGN, PRODUCTION, AND VALIDATION OF TENSION SENSORS

1.1 REQUIRED CONSTRUCTS

A variety of tension sensors have been successfully incorporated into several proteins of interest. A partial list of proteins includes vinculin (Grashoff et al., 2010), E-cadherin (Borghi et al., 2012), PECAM (Conway et al., 2013), actinin (Meng & Sachs, 2011), and spectrin (Meng & Sachs, 2012). The creation of FRET-based tension sensors requires that a tension sensing module (TSMod, Figure 1) be placed within the target protein between two domains capable of bearing force. This TSMod consists of two fluorescent proteins connected by an extensible domain;

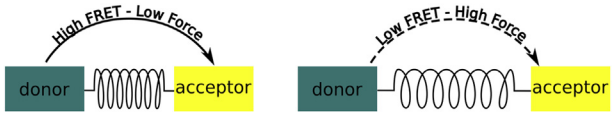

FIGURE 1

Concept of the FRET-based tension sensor. When the tension sensing module (TSMod) is not under load (left), the FRET signal is higher. When the sensor is experiencing load and the elastic linker is extended (right), the FRET signal is lower.

when load is applied to the target protein, this molecular spring extends, resulting in the separation of the fluorophores and the reduction of FRET (Figure 1). Note that no vector or directional information is reported by these sensors.

Some consideration should be taken as to the expected physiological force exerted on the protein of interest and the range of forces that can be measured by the sensor. However, this is quite challenging, as the forces associated with physiological processes are typically discussed in terms of macroscopic variables, such as shear stresses in the vasculature (Hahn & Schwartz, 2009) or compressive pressures in cartilage (Grodzinsky, Levenston, Jin, & Frank, 2000). How these mechanical stimuli are transferred to the molecular level is not clear. Furthermore, many of the various tension sensing modules are not calibrated or are only approximately calibrated in terms of the force sensitivity. Thus, several sensors may have to be evaluated to determine what is appropriate for a particular scenario. The most accurately calibrated sensor, which has been probed directly at the single molecule level (Grashoff et al., 2010), has a force sensitivity of 1−6 pN and has been shown to work in a variety of proteins, including vinculin (Grashoff et al., 2010), E-Cadherin (Borghi et al., 2012), VE-cadherin (Conway et al., 2013), and spectrin (Krieg, Dunn, & Goodman, 2014). As long as the tension sensor module is not altered (i.e. changing the fluorescent proteins or altering the extensible domain), the calibration should not need to be performed for each protein.

As not all proteins will be amenable to this insertion, a variety of control constructs (Figure 2) must be created to establish the functionality of any new tension sensor:

1. Full length tension sensor (Figure 2(B)).
2. Force-insensitive tension sensor: Enables validation that the tension sensor is indeed bearing load, through establishment of the zero-force FRET signal. These sensors can be created through a “tailless” construct which lacks a required load-bearing domain (Figure 2(C)) or by placing the TSMod at the terminus of the protein of interest (not shown).
3. Functionality control: The protein of interest is tagged with the acceptor fluorophore such that protein function is maintained (Figure 2(D)).
4. Acceptor- and donor-internal: For proper analysis, all FRET should occur intramolecularly, across an individual TSMod. At high local densities or in proteins that dimerize, it is possible that tension sensors could be close enough to exhibit intermolecular FRET. Typical internal control constructs contain an individual donor or acceptor fluorophore inserted at the same location as the tension sensor itself (Figure 2(E) and (F)). Alternatively, similar constructs can be generated through the replacement of one of the fluorophores in the TSMod with a mutant nonfluorescent version, typically induced by simple point mutations within the original fluorescent proteins (Conway et al., 2013). In either case, these intermolecular FRET control constructs have only one functional fluorophore, and testing for the existence of intermolecular FRET is accomplished through co-transfection experiments.

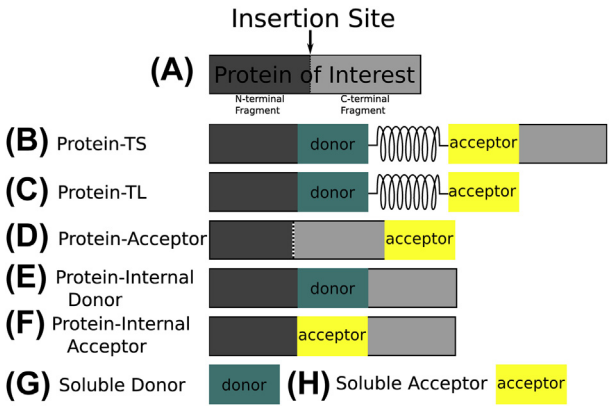

FIGURE 2

Required constructs for tension sensor evaluation and use. (A) The protein of interest, with the targeted insertion site. (B) The tension sensor protein (Protein-TS) is constructed by inserting the TSMod into the insertion site of the protein of interest. (C) The force-insensitive "tailless" (TL) construct is a truncation of the construct in (B). (D) The protein of interest tagged with the acceptor fluorophore. (E and F) The intermolecular FRET control constructs, where the donor (E) and the acceptor (F) fluorophores have been inserted in the same site as the TSMod. (G and H) The soluble versions of the acceptor (G) and donor (H) fluorophores, used to control for bleed-through effects.

5. Soluble donor and acceptor: As discussed in further detail in Section 3, one of the main difficulties with the use of FRET-based tension sensors is the correction of signals not due to FRET, known as bleed-through. Bleed-through correction requires constructs containing the individual soluble donor and acceptor fluorophores (Figure 2(G) and (H)).

1.2 MATERIALS FOR TENSION SENSOR CREATION

- TE buffer (Tris-EDTA buffer, pH 8.0, Mediatech, 46-009)
- Nuclease-free water (Sigma Aldrich, W4502)
- DNA oligonucleotides (10 μM)
- Purified plasmids containing cDNA of the target protein, TSMod, donor and acceptor proteins. Typical host vectors include pcDNA3.1 (Life Technologies) or smaller cloning vectors, such as pBluescript SK (Agilent).
- Phusion High-Fidelity DNA Polymerase and associated HF and GC buffers (New England Biolabs, M0530L)
- Deoxyribonucleotide triphosphate mix (dNTPs, 10 mM)
- Restriction enzymes, T4 DNA ligase, and respective buffers (New England Biolabs)
- Equipment to run agarose gels (Bio Rad, 170-4487)
- Agarose gel extraction kit (Qiagen, 28704)
- 1 kb DNA ladder (Bioline, 33053)

- 100% dimethyl sulfoxide (DMSO, New England Biolabs, B0515)
- DpnI (New England Biolabs, R0176L)
- Chemically competent cells (MAX-efficiency DH5α, Life Technologies, 18258)
- If using method 3: Gibson Assembly® Cloning Kit (New England Biolabs, E5510S)

1.3 DESIGN AND PRODUCTION OF CONSTRUCTS

The design of a tension sensor begins with the selection of an appropriate insertion site for the TSMod (Figure 2(A)). Several factors guide the selection of this location, and efforts are greatly simplified if the crystal structure and/or domain organization of the target protein are known. First, a literature search should be conducted, identifying functional domains and amino acids known to facilitate protein localization or functionality of the target protein. Portions of the protein that are relatively unstructured, clear of known protein binding domains, lack critical phosphorylation sites, and are between at least two load-bearing domains are viable spots for inclusion of the TSMod. Insertion sites flanked by small, uncharged amino acids should be favored, as these amino acids do not contain chemical moieties likely to be critical in dictating protein structure or function. Often, several potential insertions sites will have to be attempted, as some will result in poorly expressed or nonfunctional tension sensors.

Several different molecular cloning tools are available to build the required constructs. We will discuss the use of restriction enzymes, overlap extension, and Gibson Assembly (Figure 3). Note that special care must be taken in designing the primers in all of the listed techniques as there is significant sequence homology between the fluorescent proteins commonly used in FRET. Ensure the primers made are long enough to bind to nonhomologous regions. Typically, this requires at least 30 base pairs.

1.3.1 Restriction enzyme-based cloning

This approach takes advantage of the polymerase chain reaction (PCR) to create three DNA fragments containing compatible and unique restriction enzyme (RE) recognition sequences (RSs) at their termini. Briefly, this process involves placement of the same two RSs (RS2 and RS3) at the ends of the TSMod and in the cDNA of the target protein at the intended insertion site (Figure 3(A)). This method relies on the identification of four RSs not present in the target protein or plasmid. The advantage of this approach is its simplicity as long as proper RSs can be identified. A drawback is that the resulting tension sensor will have additional amino acids as encoded by RS2 and RS3, i.e. a "cloning scar." The selection of which RSs to place at the ends of the protein (RS1 and RS4 in Figure 3(A)) is dictated by the multicloning site of the plasmid.

1.3.1.1 Methods

1. Design the following oligonucleotide PCR primers:
   a. Forward and reverse primers for N-terminal portion of the target protein, incorporating RS1, RS2, a leading Kozak sequence, and start codon.
   b. Forward and reverse primers for the TSMod, incorporating RS2 and RS3.

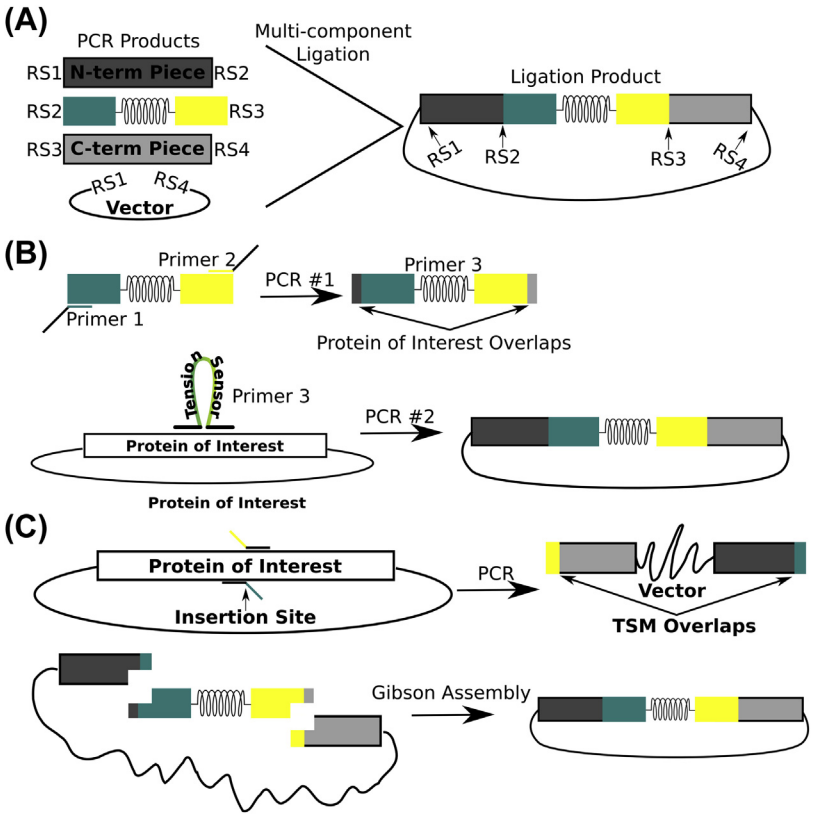

FIGURE 3

Production of tension sensor constructs. (A) With proper primer design and restriction enzyme selection, one can use PCR to create compatible fragments of cDNA from the target protein and the TSMod. A multicomponent ligation is used to reconstruct the tension sensor from these fragments, leaving "cloning scars" between the target protein and the TSMod. (B) Overlap-extension methods (Bryksin & Matsumura, 2010) can be used to build the tension sensor constructs. This method requires two PCR stages: (1) building the megaprimer, which includes the TSMod with overlaps to the protein of interest and (2) inserting this megaprimer into the protein of interest. (C) Gibson Assembly can also be used to build tension sensors and requires creation of several PCR products with overlaps between the intended insertion site and the TSMod. A series of enzymatic reactions then combine the products (Gibson et al., 2009). While we typically use a guideline of 60 s/kb of DNA, the extension time is determined by the length of the final product (vector, target protein, and TSMod) as well as the polymerase being used.

c. Forward and reverse primers for the C-terminal portion of the target protein, incorporating RS3 and RS4 and a stop codon.

2. Prepare PCR reaction mixtures for N-terminal and C-terminal portions of target protein and TSMod: All mixtures contain 4 μL HF buffer, 0.4 μL dNTPs,

0.2 μL polymerase, 1 μL forward primer, 1 μL reverse primer, 30 ng of the corresponding template DNA, and nuclease-free water to bring total volume to 20 μL.

3. Run PCR for each amplification reaction:
   a. Initial denaturation: 98 °C, 30 s
   b. Denaturation: 98 °C, 10 s
   c. Annealing: 5 °C lower than primer melting temperature, 20 s
   d. Extension: 72 °C, 60 s/kb
   e. Final extension: 72 °C, 300 s
   f. Typically, 30 cycles of the denaturation, annealing and extension phases are sufficient.
4. Run PCR products and a DNA ladder on a 1% agarose gel and ensure that the bands are the appropriate length. Cut appropriate bands and extract DNA fragments using the gel extraction kit.
5. Digest plasmid and PCR products with the REs previously designed into the primers (Figure 3): Reactions typically contain 1 μL of each RE, 2 μL of the appropriate 10X buffer, and nuclease-free water to bring the final volume to 20 μL.
6. Run the digested PCR products and plasmid on a 1% agarose gel and extract the bands using the gel extraction kit.
7. Ligate the fragments together using reaction mixture: 2 μL 10X buffer, 1 μL T4 DNA Ligase, PCR fragments, and plasmid. Use nuclease-free water to bring total volume to 20 μL.
   a. Several molar ratios of fragments are likely to work, but we have had success with a molar ratio of 4:4:4:1 of the three fragments and target plasmid. Online tools, such as the biomath tools hosted by Promega, can aid in this calculation. In addition, 50 ng of the target plasmid should be sufficient.
8. Transform 1−4 μL of ligation reaction into competent cells following manufacturer's guidelines.
9. Amplify and isolate DNA through standard protocols.

1.3.2 Megaprimer-based overlap extension

This RE-free approach enables insertion of the TSMod into the target protein at a particular position without forming a cloning scar (Bryksin & Matsumura, 2010). It is based on the creation of a megaprimer composed of the TSMod with overhangs homologous to the desired insertion site in the target protein (Figure 3(B)). In a PCR reaction with a plasmid containing the target protein, the overhangs will anneal at the insertion region and amplify the entire plasmid.

1.3.2.1 Methods

1. Design the following primers:
   a. Forward primer (Primer 1 in Figure 3(B)): This primer should be ~60 bp in length and contain a ~30 bp region corresponding to the sequence of the

target protein upstream of the insertion site. The last ~30 bp should correspond to the 3'-end of the donor fluorophore.

b. Reverse primer (Primer 2 in Figure 3(B)): This primer should be ~60 bp in length and contain a ~30 bp region corresponding to the sequence of the target protein downstream from the insertion site. The last ~30 bp should correspond to the 5'-end of the acceptor fluorophore.

2. To generate the megaprimer (Primer 3 in Figure 3(B)), perform a PCR reaction with the primers described, using a suitable plasmid containing TSMod as the template DNA. The reaction mixture should contain 10 μL 5X Phusion buffer, 1 μL 10 mM dNTP, 2.5 μL 10 μM forward primer, 2.5 μL 10 μM reverse primer, 2.5 μL DMSO, 0.5 μL Phusion polymerase, template DNA, and nuclease-free water to bring total volume to 50 μL. Due to the large size of the primers and this high melting temperature, we typically use a slightly simplified PCR cycle, in which annealing and extension both occur at 72 °C:

a. Initial denaturation: 98 °C, 30 s
b. Denaturation: 98 °C, 30 s
c. Annealing and extension: 72 °C, 60 s/kb
d. Final extension: 72 °C, 300 s
e. Twenty cycles of denaturation, annealing, and extension is usually sufficient to obtain amplification.

3. Run the PCR products and a DNA ladder on a 1% agarose gel and extract the appropriately sized DNA fragment using a gel extraction kit.

4. Perform a second PCR that will result in the insertion of the megaprimer within the target protein. Here, it is critical that the megaprimer be used in large excess, typically a 250:1 M ratio of megaprimer to vector. The reaction mixture should include 10 μL Phusion buffer, 1 μL 10 mM dNTP, megaprimer, 2.5 μL DMSO, 0.5 μL Phusion polymerase, template DNA, and nuclease-free water to bring total volume to 50 μL. A typical PCR program is:

a. Denaturation: 98 °C, 30 s
b. Annealing: 60 °C, 30 s
c. Extension: 72 °C, 60 s/kb
d. Thirty cycles are typically sufficient.

5. After PCR, use DpnI to digest the template plasmid, then heat-inactivate DpnI at 80 °C for 20 min.

6. Transform 1−4 μL of this reaction mixture into competent cells following manufacturer's guidelines.

7. Amplify and isolate DNA through standard protocols.

1.3.3 Gibson assembly

Gibson Assembly allows for the joining of arbitrary DNA sequences through the careful design of PCR primers and the use of a multifunctional cocktail of enzymes, which includes T5 exonuclease, Phusion polymerase, and Taq ligase. The mechanistic details are beyond the scope of this article but are fully detailed elsewhere (Gibson et al., 2009). Like overlap extension, this technique produces tension

sensors lacking cloning scars (Figure 3(C)). Another advantage of this technique is the availability of Gibson Assembly kits such as those available from New England Biolabs, making this technique feasible for even novice users.

1.3.3.1 Methods

1. Design primers to amplify and add overlap regions to the TSMod and your gene of interest plasmid:
   a. Forward and reverse primers for the gene of interest: These primers should be targeted to amplify the entire plasmid starting from the TSMod insertion site. They should also add ~30 bp overlap regions, which match the flanking TSMod sequences.
   b. Forward and reverse primers for the TSMod: These primers will be very similar to those used for overlap extension with the addition of ~20 bp of overlap with the regions flanking the insertion site.
2. Prepare PCR reaction mixtures to amplify gene of interest and TSMod: All mixtures are of 50 μL total volume and contain 10 μL HF buffer, 1 μL dNTPs, 0.5 μL polymerase, 2.5 μL forward primer and 2.5 μL reverse primer, and the appropriate template DNA.
3. Run PCR for each amplification reaction:
   a. Initial denaturation: 98 °C, 30 s
   b. Denaturation: 98 °C, 10 s
   c. Annealing: 5 °C lower than primer melting temperature, 20 s
   d. Extension: 72 °C, 60 s/kb
   e. Final extension: 72 °C, 300 s
   f. Typically, 30 cycles of the denaturation, annealing, and extension phases are sufficient.
4. Run the PCR products and a DNA ladder on a 1% agarose gel, ensuring that the length of the PCR products is correct. Extract the bands with a gel extraction kit.
5. Run the Gibson Assembly reaction according to the directions provided by New England Biolabs
6. Transform 1−4 μL of assembly reaction into competent cells following manufacturer's guidelines.
7. Amplify and isolate DNA through standard protocols.

1.4 BIOCHEMICALLY VALIDATING A TENSION SENSOR

The creation of a novel tension sensor requires the incorporation of two fluorescent proteins within the target protein. A properly functioning tension sensor must have a behavior indistinguishable from endogenous protein. While several tension sensors have been created, not all target proteins will maintain function after insertion of the TSMod. The location of the insertion site can dramatically affect a sensor's ability to recapitulate endogenous protein function. While the tests required to validate a

tension sensor will be dependent on the target protein, a minimal set of experiments is recommended (Grashoff et al., 2010):

- Perform sodium dodecyl sulfate -polyacrylamide gel electrophoresis and Western Blot analysis to ensure that the tension sensor is expressed at the expected molecular weight and is not subject to degradation.
- Use immunocytochemical analysis with validated antibody to show that localization of tension sensor and endogenous protein are identical.
- Conduct fluorescence recovery after photobleaching (FRAP) experiments comparing the acceptor fluorophore-tagged target protein (functionality control construct) and the tension sensor to show that the dynamic properties of target protein are maintained.
- Complete co-immunoprecipitation assays to show that interactions with known binding partners are maintained with the tension sensor. Critical interactions that are near the insertion site of the TSMod are especially important to verify.
- If possible, it should be demonstrated that the tension sensor is capable of restoring a cellular function that is lost upon lack of expression of the endogenous target protein. Previously generated tension sensors have rescued the ability of cells to respond to the application of shear stress (Conway et al., 2013) or to adhere to neighboring cells (Borghi et al., 2012).

2. IMAGING OF FRET-BASED BIOSENSORS

The intricacies associated with proper imaging and analysis of FRET-based tension sensors often prevent their widespread use. This is partially because there is no single protocol for imaging and analyzing these sensors, as they vary with the design of the biosensor as well as the type and setup of the microscope. Here we discuss approaches that are used for unimolecular FRET-based biosensors, as this is the design required for a tension sensor, and single-camera widefield microscopy. Due to the prevalence of the required equipment, relative ease of the technique, and compatibility with high-rate imaging over large areas, we focus on sensitized emission methods for detecting FRET.

2.1 KEY CONCEPTS OF FRET IMAGING

In the simplest terms, to quantify FRET, we need an estimate of donor emission and acceptor emission in response to light capable of exciting the donor fluorophore. These are commonly referred to as the donor and FRET channels, respectively. Additionally, we often measure acceptor emission in response to light that will selectively excite the acceptor fluorophore, known as the acceptor channel. This signal is independent of FRET and is directly proportional to the concentration of unimolecular FRET probes. For FRET to occur, there must be overlap in the wavelengths that the donor emits and the acceptors absorbs photons (Figure 4). This proximity often leads to mixing or contamination between the imaging channels. Bleed-through

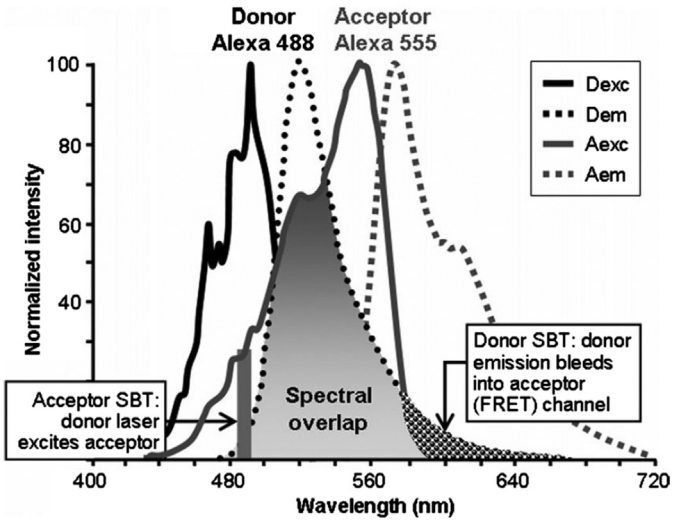

FIGURE 4

Bleed-through and cross-talk. Quantitative FRET measurements require spectral bleed-through (SBT) correction. FRET's requirement for spectral overlap occurs at the expense of SBT. Significant spectral overlap (gray shaded area) between donor (ex. AlexaFluor 488) emission and acceptor (ex. AlexaFluor 555) excitation is essential for the occurrence of FRET. Acceptor SBT occurs when the donor excitation wavelength (488 nm, gray vertical bar) excites acceptor fluorophores, increasing signal in the FRET-channel. Donor SBT occurs when the donor emission increases signal in the FRET channel (black/white circles). Dexc = Donor absorption wavelength spectrum; Aexc = Acceptor absorption wavelength spectrum; Dem = Donor emission wavelength spectrum; Aem = Acceptor emission wavelength spectrum.

Figure and caption modified from Periasamy, Wallrabe, Chen, and Barroso (2008).

typically refers fluorescence due to a single fluorophore appearing in the FRET channel. This can be due to the donor fluorophore emitting light at acceptor wavelengths or donor excitation light also stimulating the acceptor fluorophore. Cross-talk typically refers to the respective fluorophores causing signal in each other's channels (i.e. the donor fluorophore causing a signal in the acceptor channel or vice versa) and is often insignificant with properly designed filters.

2.2 MATERIALS AND EQUIPMENT

2.2.1 Reagents

- Glass-bottom Petri dishes (35 mm diameter, 0.17 mm thickness, World Precision Instruments Inc.)
- Fluorescent microspheres of desired size and fluorescence, which will vary depending on objective properties and FRET pair, respectively. For the

Teal−Venus FRET pair, two sets of microspheres are required: (1) 0.5 μm TetraSpeck™ microspheres (Life Technologies, T7281) and (2) 0.5 μm Fluoresbrite® YG microspheres (Polysciences Inc., 17152-10). Details on microsphere selection and use can be found in Section 2.3.2

- Phosphate buffered saline (PBS): 137 mM NaCl, 2.7 mM KCl, 10 mM Na_2HPO_4, 2 mM KH_2PO_4, pH to 7.2−7.4 with HCl
- Human fibronectin (Fisher Scientific, CB-40008A)
- Growth medium: DMEM, high glucose (Sigma Aldrich, D6429) supplemented with 1X non-essential amino acids (Life Technologies, 11140), 10% FBS (HyClone), 1X Antibiotic Antimycotic Solution (Sigma Aldrich, A5955)
- Transfection reagents: Plasmid DNA constructs, Lipofectamine 2000 (Life Technologies, 11668), OptiMEM I (Life Technologies, 11058)
- Imaging medium: Medium 199, without phenol red, which contains sodium bicarbonate for pH buffering (Life Technologies, 11043) supplemented with 10% FBS (HyClone)
- Immersion Oil (Cargille, Type LDF)

2.2.2 Equipment

- Inverted fluorescence microscope (Olympus, IX83)
- Xenon arc lamp (Sutter Instruments, Lambda LS)
- Objective (Olympus, UPlanSApo-60X, 1.35NA oil immersion)
- Motorized filter wheels (Sutter Instruments, Lambda 10-3)
- Automated Stage (Prior, H117EIX3)
- Vibration damping laboratory table (Ametek, Technical Manufacturing Corporation, 63-500 Series)
- Digital camera (Hamamatsu, ORCA-Flash4.0 V2, C11440)
- Excitation and emission filters and dichroic mirror (depend on donor and acceptor fluorophores)
- Specimen warming system and objective heater (Bioptechs, 403-1926 and 150803)
- Image acquisition software (Metamorph Advanced, Olympus)
- Marker or diamond tip pen

2.3 PREPARATION FOR AND IMAGING OF FRET-BASED TENSION SENSORS

2.3.1 Experimental sample preparation

The tension sensors are readily expressed in common murine cell lines (e.g., mouse embryonic fibroblasts) through standard transient transfection protocols. We find that Lipofectamine 2000 utilized according to manufacturer's instruction is sufficient. Lentiviral transduction and electroporation methods are more efficient, but have their own drawbacks as additional cloning and specialized equipment are required. Typically, we use a cell line lacking endogenous expression of the protein of interest and tune expression levels to be relatively close to endogenous levels, as gauged by Western blotting (Grashoff et al., 2010).

2.3.1.1 Methods

1. Coating Glass-bottom dishes with fibronectin.
   a. Dilute fibronectin in PBS to a concentration of 0.01 mg/mL.
   b. Add 1 mL of fibronectin solution to each glass dish ($\sim$0.4 mL/cm^2).
   c. Allow dishes to incubate at 4 °C overnight.
2. Plating cells
   a. After 24–48 h of transfection, use standard methods to passage cells from 6-well dishes to fibronectin-coated glass bottom Petri dishes.
   b. Allow cells to adhere for 3–4 h before imaging.

2.3.2 Detection of common imaging artifacts

Quantitative widefield microscopy is essential for the proper use of FRET-based tension sensors and requires knowledge of and correction for a number of common imaging artifacts. Brief descriptions and methods for the assessment of these artifacts are provided in the following sections. The ultimate use of these images will be covered in detail in Section 3. (For more detailed discussions of the following points, please refer Hodgson, Shen, & Hahn, 2010; Spiering, Bravo-Cordero, Moshfegh, Miskolci, & Hodgson, 2013; Waters, 2009).

2.3.2.1 Methods

1. *Measure dark current*: Dark current is the background signal present in the camera detector when no photons are being passed to it, which changes with thermal fluctuations in the camera. Quantification of dark current enables correction for dark or "hot" pixels and is especially pronounced when using long exposure times typical in FRET imaging. Acquire approximately 10 dark-frame images in each channel under the same conditions as experimental images, but with all shutters in the microscope closed.
2. *Obtain shade correction images*: Uneven illumination, inherent to many fluorescence microscopy systems, introduces shading effects causing portions in the field of view to appear brighter than others. This uneven shading can be quantified by imaging glass-bottom Petri dishes, coated with fibronectin and containing imaging media, and imaged identically to experimental samples. Additionally, the focal plane should be approximately the same distance from the glass substrate, ensured by marking dishes with a marker or diamond tip pen, providing elements to focus on. Typically, 10–20 shade correction images are taken in each channel.
3. *Measure three-dimensional offsets in multiple channels*: Due to multiple reasons, including chromatic aberrations and small hardware misalignments, physically co-localized objects may appear offset in images. Imaging fluorescent microspheres that appear in multiple channels can be used to measure and then correct for these shifts. Due to variations in the thickness and flatness of microscopy dishes and microscope stages, it is commonly held that this type of estimate must be done for every image. While this is the preferred

method, we have found that by using commercially produced glass bottom Petri dishes and consistently leveling the stage, highly reproducible estimates of the three-dimensional offsets needed to register any number of fluorescent channels can be made. Unfortunately, there are no commercially available fluorescent microspheres that appear in all three imaging channels used for Teal−Venus tension sensors. Alignment of donor and FRET channels is crucial for accurate FRET index calculations and requires Fluoresbrite® YG microspheres. To estimate measurement accuracy and ensure the alignment algorithms are working correctly, we also use TetraSpeck™ microspheres to align acceptor and FRET channels, which have the same emission filter and thus should be perfectly aligned. Due to differences in brightness between these two types of microspheres, mixing them in one sample is not recommended. Ultimately, we are able to measure optimal focal plane, X−Y translational shifts, and radial corrections necessary to align images required for FRET analysis.

a. Dilute fluorescent microspheres in PBS (Fluoresbrite® YG microspheres require 1:10,000 dilution v/v).
b. Place 10 μL drops of the diluted microspheres in several locations on a glass bottom dish. Allow liquid to evaporate overnight.
c. After PBS has completely evaporated, rinse the dish three times with PBS, leaving the microspheres covered with PBS after the final rinse.
d. Place dish on microscope, taking special care to make sure dish is flat with respect to the objective. This is often done through the use of levels and the imaging system itself. In a properly leveled system, structures should exit the focal plane simultaneously as the focal plane is altered. Thus, the user can manually determine sample flatness by focusing up and down and ensuring that all objects come into focus simultaneously. The appearance of microspheres coming into focus as a "wave" is indicative of a slanted coverslip. However, as this process may be time intensive, use low levels of illumination and during an experiment, do not image cells for sample leveling in the same area as for FRET imaging.
e. Take a Z-stack made up of 21 images with a step size of 100 nm (∼1/5 the diameter of the microspheres) acquiring images in donor and FRET channels.
f. Acquire 5−10 image stacks taken from multiple positions in the sample.
g. Repeat (steps a to f) using TetraSpeck™ microspheres at a 1:10 dilution and image acceptor and FRET channels.

2.3.3 Imaging of tension sensors and control constructs

Here we describe general considerations for imaging of FRET-based tension sensors. The analysis of these images will be discussed in Section 3. While methods for detection of and correction for common imaging artifacts have been outlined in detail, it is always necessary to prepare a host of controls in order to definitively draw conclusions from FRET-based tension sensor experiments. To conduct a

complete FRET experiment, prepare cells transfected with each of the constructs outlined in Section 1.1 (Figure 2).

2.3.3.1 Methods

1. Preparation:
   a. Turn on fluorescence light source (arc lamp) and stage-heating apparatus at least 1 h before imaging begins, allowing system to reach a stable state.
   b. Remove growth media, wash cells once with PBS, and add imaging medium. This is critical to achieving a higher signal-to-noise ratio, as phenol red is a fluorescence quencher and some components of DMEM, especially riboflavin, exhibit significant autofluorescence in FRET channels (Vishwanath & Ramanujam, 2000). Alternatively, cells could be re-suspended in imaging media during re-plating.
   c. Place cells on prewarmed microscope stage, and allow to thermally equilibrate for 10–20 min before imaging.
2. *Imaging proper focal plane*: Having previously measured the focal plane shift between channels, it is important to use an automated stage to properly focus on donor, acceptor, and FRET channels. Metamorph's Multi-Dimensional Acquisition plugin includes a "Journals" option, with which it is possible to program the stage to adjust focus between specific wavelengths with a minimum step size of 10 nm.
3. *Bleed-through image acquisition*: Use cells transfected with soluble donor and acceptor fluorophores and identical settings to those used in the experimental groups to acquire 10–20 bleed-through images for both donor and acceptor. Select cells such that the full spatial and intensity range of the digital camera is probed.
4. *Experimental image acquisition settings*: While searching for cells, we often use a 10% neutral density (ND) filter to minimize photobleaching and phototoxicity. Reagents such as Oxyrase or other free-radical scavengers can be used as well, but may be too harsh for imaging lasting more than a timescale of minutes. Typical exposure times used to image a vinculin tension sensor with a 60× objective are 500–1500 ms while using either a 50% or 100% ND filter. Reasonably long exposures with lower intensity are preferable over short exposures to high intensity light (Hodgson et al., 2010).

3. METHODS OF ANALYSIS OF FRET IMAGES

3.1 QUANTIFICATION AND CORRECTION OF COMMON IMAGING ARTIFACTS

The major goals of image processing for FRET experiments are the following: enhance the signal-to-noise ratio, remove artifacts due to the imaging system,

correct for bleed-through between different imaging channels, and calculate FRET index. We use custom code, available upon request, written in MATLAB (Mathworks) to perform all of these steps, but software packages are available. Our basic image analysis protocol is outlined in Figure 5.

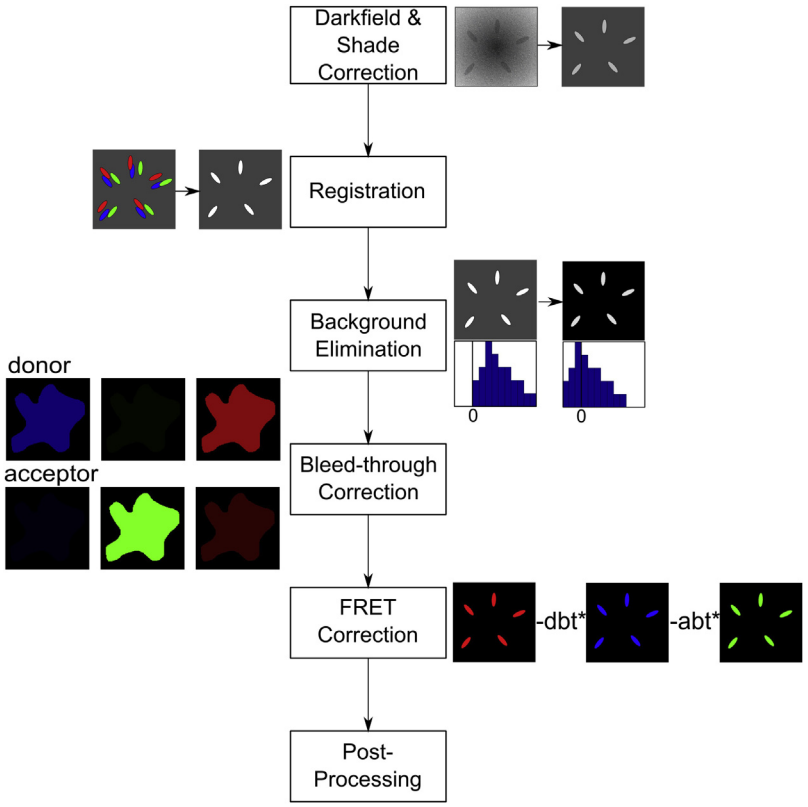

FIGURE 5

Image processing for FRET-based biosensors. This schematic summarizes the image processing steps taken to remove general imaging and FRET artifacts and then calculate FRET index values. First, remove dark current and correct for uneven illumination in all images. Then, account for X–Y translational shifts between imaging channels by registering the images to a reference channel. Next, use histogram-based methods to remove the background intensity from each image. For FRET correction, measure the bleed-through and cross-talk between the imaging channels using images taken of cells expressing single fluorophores. Use these bleed-through values to correct the experimental images and calculate the FRET index values. Post-processing, including segmentation and statistical analysis, is performed on these fully corrected images. Blue = donor channel (dark gray in print versions); green = acceptor channel (white in print versions); red = FRET channel (gray in print versions).

3.1.1 Methods

1. *Dark current subtraction*: Dark frame images are averaged together and subtracted from all other images in the data set, including the shade correction images.
2. *3D image registration*: Imaging fluorescent microspheres in a Z-stack allows for the precise measurement of both translational shifts (X−Y plane) and differences in focal plane (Z-shifts) between fluorescent channels simultaneously. It is important to verify that calculations and corrections are properly registering images; this can be accomplished by overlaying the images in ImageJ (Figure 6). The following registration protocol first requires user-determined measurement of proper focal plane so that X- and Y-shifts can be calculated from "in focus" images. Channel-dependent differences in focal plane are often minimal (<100 nm) for super-apochromatic objectives, especially in the green-red wavelengths often used with FRET sensors.
   a. Calculate focal plane, X-shift and Y-shift
      - Load a reference image, focused on by the user (we use the FRET channel).
      - Load the stack of donor channel images (Figure 7(A)) and compare each slice in the stack to the reference image by cross-correlation analysis (Guizar-Sicairos, Thurman, & Fienup, 2008).
      - This computationally efficient subpixel registration algorithm is used to calculate the root-mean-square error (RMSE) between the two input images, along with the X−Y translational shifts necessary to register them

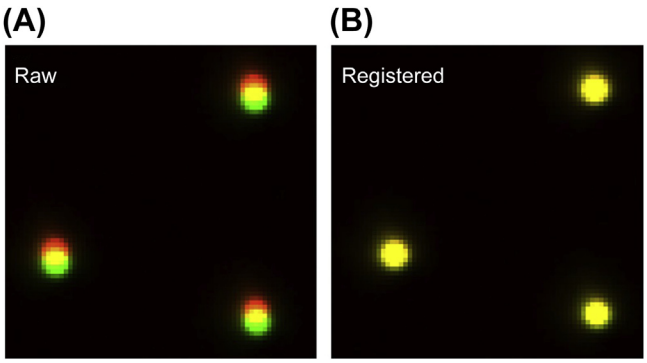

FIGURE 6

Confirmation of proper image registration. Subpixel image shifting algorithms (for example, interp2 in MATLAB) are used to align the signals from images of microspheres in different fluorescent channels. (A) Signals from spatially identical samples appear in different locations because of hardware misalignments and chromatic aberrations. (B) Proper alignment of channels can be confirmed by simple red (light gray in print versions)—green (white in print versions) overlays performed using ImageJ software.

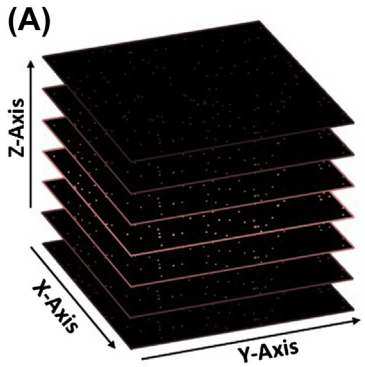

(B)

Image	Focal Plane (nm)	RMSE	X-shift	Y-shift
1	+500	0.51	-0.30	0.10
2	+400	0.41	-0.20	0.08
3	+300	0.36	-0.15	0.06
4	+200	0.32	-0.10	0.04
5	+100	0.30	-0.05	0.05
6	0	0.32	0.00	0.06
7	-100	0.38	0.05	0.07
8	-200	0.45	0.10	0.08
9	-300	0.52	0.15	0.10
10	-400	0.60	0.20	0.12
11	-500	0.70	0.30	0.14

FIGURE 7

Analyzing image stacks for 3D registration of images. (A) Use an automated stage to acquire a stack of 21 images of fluorescent microspheres in donor, acceptor, and FRET channels. (B) Subpixel registration algorithms (Guizar-Sicairos et al., 2008) can be used to calculate proper focal plane (by RMSE minimization) and X–Y translational shifts necessary to properly align donor, acceptor, and FRET channels at the predetermined focal plane. Note that these X- and Y-shifts are often not minimal at the proper focal plane.

(Figure 7(B)). Repeat for every image stack and save RMSE, X-shift, and Y-shift as a function of image number (focal plane).

- For each image stack, calculate the plane at which RMSE is minimized by cubic spline interpolation and average these calculated Z-offsets. Note that these measured Z-offsets must be taken into account during image acquisition (see Section 2.3.3 above).
- Calculate the X- and Y-shifts at the proper Z-offset. We have found that the Teal–Venus imaging channels for our setup require subpixel shifts.
- Repeat for acceptor channel images to determine measurement accuracy (acceptor and FRET channels should co-localize perfectly since they have identical emission wavelengths).

b. Register experimental images

- Input the shifts that have been calculated previously for each of the donor, acceptor, and FRET channels.
- Use a subpixel accurate 2D interpolation to shift each of the bleed-through and experimental images to the calculated shifted positions for the particular channel.
- Crop the edges of the image to eliminate edge effects. The number of pixels to take off from the edge should exceed your largest translational shift

3. *Radial distortion correction*: The typically small radial distortions present in many imaging systems can affect FRET imaging. These can be measured with particle tracking algorithms (Crocker & Grier, 1996) and corrected with

software after processing (Vass & Perlaki, 2003). Details can be obtained by contacting the authors of this paper.

4. *Shade correction*:
   a. Load and average 10−20 shading images for each channel.
   b. Fit each averaged shade image with a 2D quadratic surface to eliminate effects due to spurious pixels or local artifacts.
   c. Normalize each shading surface to its maximum value.
   d. For each imaging channel, divide all other images in the data set by the corresponding normalized averaged shading surface.
5. *Background subtraction*: To enhance the signal-to-noise ratio, we subtract the background noise from each individual image. As cells are sparsely plated, we use histogram-based methods to estimate background as the mode of each image (Gonzalez & Woods, 2008).
6. *Bleed-through calculation*: To extract the FRET index values from experimental images, the amount of signal in the FRET channel due to bleed-through must be measured. In our system, bleed-throughs do not depend on intensity, and cross-talk between the donor and acceptor channels is zero.
   a. Load in images taken of cells transfected with soluble acceptor fluorophore only and soluble donor fluorophore only, analyzed according to the previous steps.
   b. For each channel in the acceptor-only and donor-only samples, sort all pixels in the image and bin them by intensity. Average the pixels within each bin.
   c. To find the acceptor bleed-through, fit a linear curve to the relationship between the FRET intensity in each bin to the acceptor intensity. The slope of this fit is the acceptor bleed-through. Follow an analogous procedure for calculating the donor bleed-through.
   d. To find the cross-talks, repeat step c, but use the non-FRET channel intensity in place of the FRET channel intensity.
7. *FRET correction and generation of FRET index*: Estimates of the amount of bleed-through can be used to calculate the FRET index values. To speed image processing, we discard pixels barely indistinguishable from the background ($<1\%$ of maximum signal).
   a. Load in donor, acceptor, and FRET experimental images, analyzed according to the previous steps.
   b. To remove bleed-through, subtract the acceptor bleed-through multiplied by the acceptor channel image and the donor bleed-through multiplied by the donor channel image from FRET image.
   c. For systems that have nonzero cross-talk between donor and acceptor channels, first ensure you are using a filter set appropriate for FRET imaging as this should not occur with standard fluorescent proteins. Otherwise, the imaging protocol and analysis outlined by Chen et al. (Chen, Puhl, Koushik, Vogel, & Ikeda, 2006) can be used to simultaneously remove bleed-through and cross-talk.

d. Divide the corrected FRET image by the acceptor channel image to normalize to the concentration of the sensor and calculate the FRET index. FRET index is inversely proportional to the force on the sensor.

8. *Post-Processing*: Post-processing is highly dependent on the user's needs. For constructs that localize to areas within the cell, segmentation is useful to isolate the areas of interest. We use a segmentation protocol known as "water" to isolate focal adhesions (Zamir et al., 1999). Once identified, the regions can be quantified (e.g., position, size, intensity, orientation, axial ratio) across multiple channels.

3.1.2 Results

Figure 8 provides an example of completed vinculin tension sensor (VinTS) FRET analysis with post-processing. The donor image (Figure 8(A)) and the acceptor image (Figure 8(B)) are corrected for dark current, X- and Y-shifts, shading, and background intensity. The completely corrected FRET image is normalized to the acceptor image to remove effects of protein concentration (Figure 8(C)). Areas

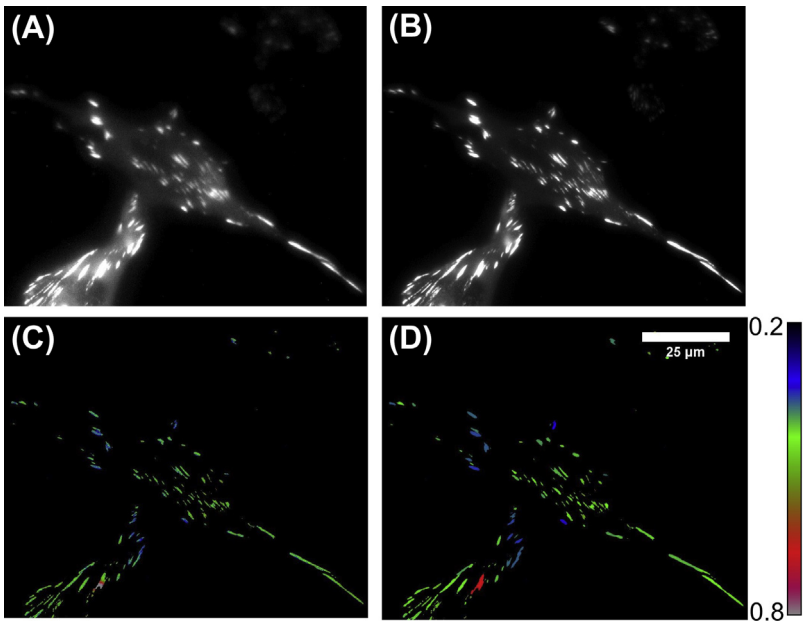

FIGURE 8

Sample vinculin tension sensor (VinTS) image. A corrected image of a cell expressing the VinTS construct in the (A) donor imaging channel and (B) acceptor imaging channel. (C) An image of FRET index in focal adhesions from the same cell, segmented using the acceptor channel image. All other pixels are set to zero. (D) FRET index values can be averaged, giving one FRET index value to each adhesion. Note that FRET is lower, and thus force is higher across VinTS, at the leading edge of the cell.

outside of segmented focal adhesions are set to zero, and within focal adhesions FRET index values are averaged together, giving one value to each adhesion (Figure 8(D)). This type of post-processing allows easy visualization of spatial patterns of vinculin tension within a cell.

3.2 EXAMPLES OF COMMON ERRORS IN FRET IMAGING

Many of the artifacts that arise from improper image analysis of FRET-based tension sensors are easily identified by visual inspection. It is always a good idea to test your

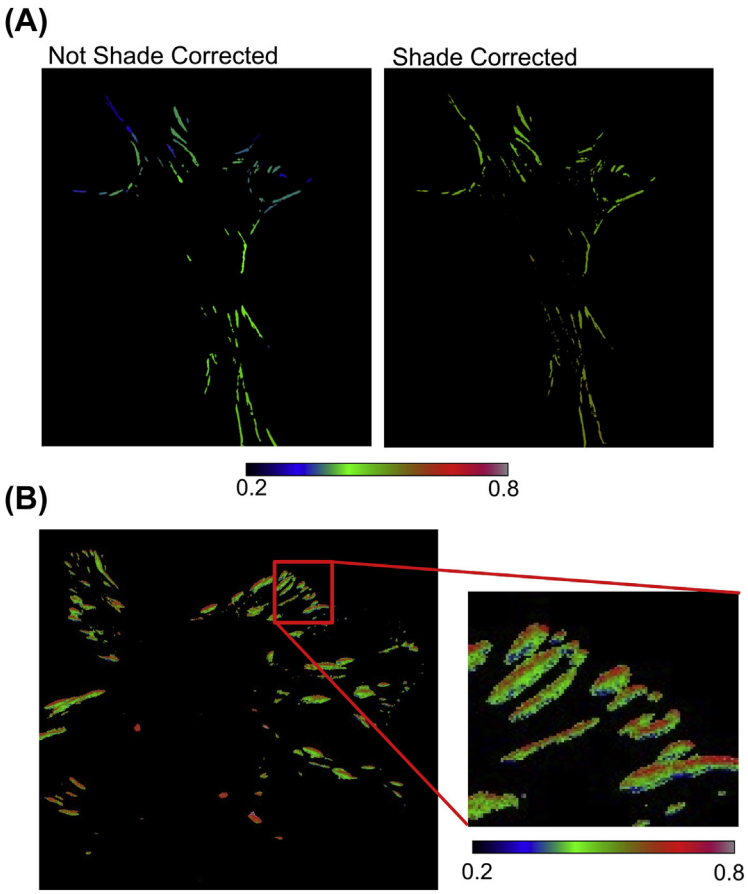

FIGURE 9

Visualization of imaging defects. (A) An image of FRET index for a cell expressing the VinTL construct (force-insensitive control) with and without shade correction. There should be no spatial variation in VinTL signal. (B) An image of FRET index for a cell expressing the VinTL construct in which the images were not registered. Artifacts exist along the edges of the focal adhesions due to misalignment of the imaging channels.

image analysis protocol on control samples, such as fluorescent microspheres or a control construct to look for these errors.

Shade correction is important for maintaining the "flatness" of the imaging field. To test this, compare the same normalized FRET index image for the force-insensitive control construct (VinTL) with and without shade correction (Figure 9(A)). The force-insensitive construct should have a uniform FRET index throughout the whole cell due to its inability to be extended. Without shade correction, there is a distinct spatial variation in FRET index that is easily detected by visual inspection.

Failing to register the different channels can result in edge artifacts (from X and Y shifts) or focus issues (from Z shifts). Improper registration of FRET images results in visible artifacts along the edges of the focal adhesions (Figure 9(B)). Again, check for gradients in FRET index in images of the force-insensitive control (VinTL). It is important to check for edge effects before masking and post-processing, as these manipulations could smooth out these artifacts, resulting in misleading data.

4. SUMMARY

FRET-based tension sensors have proven to be useful tools for measuring intracellular forces, and provide a unique view into mechanosensitive processes. Advances in molecular cloning now allow for easy and seamless construction of new tension sensors, and fundamental design criteria compiled from a number of foundational studies exist. The successful use of novel tension sensors will enable improved understanding of the mechanical basis of important cellular processes, such as migration and differentiation, as well as cell behavior in response to altered environmental conditions encountered in disease states or synthetic biomaterials.

To enable rapid imaging over a whole cell on the second to several second time scale characteristic of the signaling processes and subcellular dynamics involved in cell migration, we have described a protocol that measures FRET index. However there are some significant limitations to the outlined approach. The described technique reports a relative measure of FRET and is not easily related to the absolute separation distance of the two fluorophores. Thus this technique will report relative forces only. Measurement of absolute forces requires an absolute measure of separation distance, as determined by FRET efficiency. FRET efficiency is best measured with fluorescence lifetime imaging (FLIM) (Austen, Kluger, Freikamp, Chrostek-Grashoff, & Grashoff, 2013). This is a specialized technique that requires advanced equipment and has limited temporal resolution, as it is based on single photon counting. For instance, measurement times for a whole cell can range from tens of seconds to a minute. Nevertheless, new advances are consistently enabling improvements in FLIM microscopy (Digman, Caiolfa, Zamai, & Gratton, 2008), and in the near future, measurements of the distribution of absolute forces across a whole cell or

multiple cells at rates relevant to cell migration and the dynamics of sub-cellular structures will be possible.

REFERENCES

Austen, K., Kluger, C., Freikamp, A., Chrostek-Grashoff, A., & Grashoff, C. (2013). Generation and analysis of biosensors to measure mechanical forces within cells. *Methods in Molecular Biology, 1066*, 169–184. http://dx.doi.org/10.1007/978-1-62703-604-7_15.

Borghi, N., Sorokina, M., Shcherbakova, O. G., Weis, W. I., Pruitt, B. L., Nelson, W. J., et al. (2012). E-cadherin is under constitutive actomyosin-generated tension that is increased at cell-cell contacts upon externally applied stretch. *Proceedings of the National Academy of Sciences of the United States of America, 109*(46), 19034. http://dx.doi.org/10.1073/pnas.1217417109.

Bryksin, A. V., & Matsumura, I. (2010). Overlap extension PCR cloning: a simple and reliable way to create recombinant plasmids. *Biotechniques, 48*(6), 463–465. http://dx.doi.org/10.2144/000113418.

Chen, H., Puhl, H. L., 3rd, Koushik, S. V., Vogel, S. S., & Ikeda, S. R. (2006). Measurement of FRET efficiency and ratio of donor to acceptor concentration in living cells. *Biophysical Journal, 91*(5), L39–L41. http://dx.doi.org/10.1529/biophysj.106.088773.

Conway, D. E., Breckenridge, M. T., Hinde, E., Gratton, E., Chen, C. S., & Schwartz, M. A. (2013). Fluid shear stress on endothelial cells modulates mechanical tension across VE-cadherin and PECAM-1. *Current Biology, 23*(11), 1024–1030. http://dx.doi.org/10.1016/j.cub.2013.04.049.

Crocker, J., & Grier, D. G. (1996). Methods of digital video microscopy for colloidal studies. *Journal of Colloid and Interface Science, 179*, 298–310.

Dembo, M., & Wang, Y. L. (1999). Stresses at the cell-to-substrate interface during locomotion of fibroblasts. *Biophysical Journal, 76*, 2307–2316.

Digman, M. A., Caiolfa, V. R., Zamai, M., & Gratton, E. (2008). The phasor approach to fluorescence lifetime imaging analysis. *Biophysical Journal, 94*(2), L14–L16. http://dx.doi.org/10.1529/biophysj.107.120154.

Gibson, D. G., Young, L., Chuang, R. Y., Venter, J. C., Hutchison, C. A., 3rd, & Smith, H. O. (2009). Enzymatic assembly of DNA molecules up to several hundred kilobases. *Nature Methods, 6*(5), 343–345. http://dx.doi.org/10.1038/nmeth.1318.

Gonzalez, R. C., & Woods, R. E. (2008). *Digital image processing* (3rd ed.). Pearson Education.

Grashoff, C., Hoffman, B. D., Brenner, M. D., Zhou, R., Parsons, M., Yang, M. T., et al. (2010). Measuring mechanical tension across vinculin reveals regulation of focal adhesion dynamics. *Nature, 466*(7303), 263–266. http://dx.doi.org/10.1038/nature09198.

Grodzinsky, A. J., Levenston, M. E., Jin, M., & Frank, E. H. (2000). Cartilage tissue remodeling in response to mechanical forces. *Annual Review of Biomedical Engineering, 2*, 691–713. http://dx.doi.org/10.1146/annurev.bioeng.2.1.691.

Guizar-Sicairos, M., Thurman, S. T., & Fienup, J. R. (2008). Efficient subpixel image registration algorithms. *Optics Letters, 33*(2), 156–158.

Hahn, C., & Schwartz, M. A. (2009). Mechanotransduction in vascular physiology and atherogenesis. *Nature Reviews Molecular Cell Biology, 10*(1), 53–62. http://dx.doi.org/10.1038/nrm2596.

Harris, A. K., Wild, P., & Stopak, D. (1980). Silicone rubber substrata: a new wrinkle in the study of cell locomotion. *Science, 208*(4440), 177−179.

Hodgson, L., Shen, F., & Hahn, K. (2010). Biosensors for characterizing the dynamics of rho family GTPases in living cells (Chapter 14), Unit 14 11 *Current Protocols in Cell Biology*, 11−26. http://dx.doi.org/10.1002/0471143030.cb1411s46.

Hoffman, B. D. (2014). The detection and role of molecular tension in focal adhesion dynamics. *Progress in molecular biology and translational science, 126*, 3−24. http://dx.doi.org/10.1016/B978-0-12-394624-9.00001-4.

Hoffman, B. D., Grashoff, C., & Schwartz, M. A. (2011). Dynamic molecular processes mediate cellular mechanotransduction. *Nature, 475*(7356), 316−323. http://dx.doi.org/10.1038/nature10316.

Krieg, M., Dunn, A. R., & Goodman, M. B. (2014). Mechanical control of the sense of touch by beta-spectrin. *Nature Cell Biology, 16*(3), 224−233. http://dx.doi.org/10.1038/ncb2915.

Lakowicz, J. R. (2006). *Principles of fluorescence spectroscopy* (3rd ed.). New York: Springer.

Legant, W. R., Miller, J. S., Blakely, B. L., Cohen, D. M., Genin, G. M., & Chen, C. S. (2010). Measurement of mechanical tractions exerted by cells in three-dimensional matrices. *Nature Methods, 7*(12), 969−971. http://dx.doi.org/10.1038/nmeth.1531.

Meng, F., & Sachs, F. (2011). Visualizing dynamic cytoplasmic forces with a compliance-matched FRET sensor. *Journal of Cell Science, 124*(2), 261−269. http://dx.doi.org/10.1242/jcs.

Meng, F., & Sachs, F. (2012). Orientation-based FRET sensor for real-time imaging of cellular forces. *Journal of Cell Science, 125*(Pt 3), 743−750. http://dx.doi.org/10.1242/jcs.093104.

Meng, F., Suchyna, T. M., & Sachs, F. (2008). A fluorescence energy transfer-based mechanical stress sensor for specific proteins in situ. *FEBS Journal, 275*(12), 3072−3087. http://dx.doi.org/10.1111/j.1742-4658.2008.06461.x.

Orr, A. W., Helmke, B. P., Blackman, B. R., & Schwartz, M. A. (2006). Mechanisms of mechanotransduction. *Developmental Cell, 10*(1), 11−20. http://dx.doi.org/10.1016/j.devcel.2005.12.006.

Periasamy, A., Wallrabe, H., Chen, Y., & Barroso, M. (2008). Quantitation of protein−protein interactions: confocal FRET microscopy. *Methods in Cell Biology, 89*, 569−598. http://dx.doi.org/10.1016/s0091-679x(08)00622-5.

Plotnikov, S. V., Pasapera, A. M., Sabass, B., & Waterman, C. M. (2012). Force fluctuations within focal adhesions mediate ECM-rigidity sensing to guide directed cell migration. *Cell, 151*(7), 1513−1527. http://dx.doi.org/10.1016/j.cell.2012.11.034.

del Rio, A., Perez-Jimenez, R., Liu, R., Roca-Cusachs, P., Fernandez, J. M., & Sheetz, M. P. (2009). Stretching single talin rod molecules activates vinculin binding. *Science, 323*(5914), 638−641. http://dx.doi.org/10.1126/science.1162912.

Spiering, D., Bravo-Cordero, J. J., Moshfegh, Y., Miskolci, V., & Hodgson, L. (2013). Quantitative ratiometric imaging of FRET-biosensors in living cells. *Methods in Cell Biology, 114*, 593−609. http://dx.doi.org/10.1016/B978-0-12-407761-4.00025-7.

Tan, J. L., Tien, J., Pirone, D. M., Gray, D. S., Bhadriraju, K., & Chen, C. S. (2003). Cells lying on a bed of microneedles: an approach to isolate mechanical force. *Proceedings of the National Academy of Sciences of the United States of America, 100*(4), 1484−1489. http://dx.doi.org/10.1073/pnas.0235407100.

Vass, G., & Perlaki, T. (2003). Applying and removing lens distortion in post production. In *Proc 2nd Hungarian conf on comp graphics and geometry.*

Vishwanath, K., & Ramanujam, N. (2000). Fluorescence spectroscopy in vivo. *Encylopedia of Analytical Chemistry*, 20–56.

Waters, J. C. (2009). Accuracy and precision in quantitative fluorescence microscopy. *Journal of Cell Biology, 185*(7), 1135–1148. http://dx.doi.org/10.1083/jcb.200903097.

Zamir, E., Katz, B. Z., Aota, S., Yamada, K. M., Geiger, B., & Kam, Z. (1999). Molecular diversity of cell-matrix adhesions. *Journal of Cell Science, 112*, 1655–1669.